Effects of Texture and Triaxiality on the Plasticity of Magnesium Alloys

Balaji Selvarajou, Shailendra P. Joshi, and A. Amine Benzerga

Abstract

Understanding the role of triaxiality is key in the damage evolution of engineering alloys. In low symmetry materials, e.g. magnesium, the role of triaxiality in damage evolution is complicated by the presence of protean deformation mechanisms, which exhibit high crystallographic plastic anisotropy. We present the results of detailed finite element study of smooth and notched round bar polycrystalline specimens of magnesium, subjected to quasi-static tensile loading. Initial simulated textures mimicking and deviating from typical rolled Mg sheet textures are adopted. Using three-dimensional HCP single crystal plasticity, the effect of these textural variations is highlighted. The role of out-of-plane textural variation is compared to the in-plane variation, and the analysis indicates that out-of-plane deviations in $[10\bar{1}0]$ result in subtle changes to the macroscopic deformation anisotropy and the underlying microscopic deformation slip and twin activity. The role of these textures in the activation of twinning mechanisms is discussed. These results, in conjunction with our recent works, help develop a systematic understanding of the texture-triaxiality-anisotropy interaction in magnesium alloys.

Keywords

Stress triaxiality • Texture • Anisotropy • Crystal plasticity

Introduction

Magnesium (Mg) is an excellent candidate as a structural material, but possesses complex plastic behavior originating from its low symmetry hexagonal close packed (hcp) crystal structure. Although it has a large number of potential slip deformation mechanisms, many of them are mutually exclusive which results in a starvation of necessary number of slip systems for plastic deformation. This shortage of slip mechanisms is compensated by twinning mechanisms. Both, slip and twinning mechanisms span a wide range of critical stress regime, giving rise to high intrinsic plastic anisotropy at the single crystal level. It influences polycrystalline microstructures through textures that are dictated by processing and alloy compositions.

Understanding interaction between plastic anisotropy, texture and stress state is important from the viewpoint of designing strong and ductile Mg alloys [1–5]. Our recent works have focused on the deformation micromechanics of notched single crystal [6] and polycrystalline specimens with in-plane $(\Delta\varphi_1)$ and out-of-plane $(\Delta\varphi)$ texture effects [7]. This work extends the latter investigation by focusing on the effect of texture variation due to deviation of $[10\bar{1}0]$ out of the plane of rolled Mg sheets. In particular, we discuss the effect of stress triaxiality ($\mathcal{T} = \sigma_h/\sigma_e$ where σ_h is the

B. Selvarajou · S.P. Joshi (✉)
Department of Mechanical Engineering, National University of Singapore, Singapore, 117576, Singapore
e-mail: shailendra@nus.edu.sg

A. Amine Benzerga
Department of Materials Science and Engineering, Texas A&M University, College Station, TX 77843, USA

A. Amine Benzerga
Department of Aerospace Engineering, Texas A&M University, College Station, TX 77843, USA

K.N. Solanki et al. (eds.), *Magnesium Technology 2017*,
The Minerals, Metals & Materials Series, DOI 10.1007/978-3-319-52392-7_78

hydrostatic stress and σ_e is the von Mises equivalent stress) on the deformation micromechanics and texture evolution of Mg using three-dimensional crystal plasticity finite element calculations.

Computational Set-Up

Figure 1 shows the geometric details of smooth and notched round bar specimens that mimic experimental specimens extracted from rolled Mg sheet [1]. The smooth specimen subjected to uniaxial load corresponds to a nominal triaxiality $\mathcal{T} = 1/3$ whereas the two notched geometries correspond to $\mathcal{T}$ of about 0.6 and 0.8, respectively. Notched specimens are identified as RNξ with $\xi = 10R/D_0$ where R is the notch radius. The global X-, Y- and Z-axes of the specimens are aligned with the sheet transverse (T), rolling (L) and normal (S) directions. The geometries are discretized into a fine mesh of nearly 20,000 C3D8R finite elements.

As shown in the figure, polycrystalline structures are constructed as aggregates of finite elements such that are in a given region, finite elements are grouped together and assigned a crystallographic orientation to represent a grain. The total number of grains (N_g) is approximately the same for the three geometries. In constructing a polycrystal of certain texture, the $[10\bar{1}0]$ and $[0001]$ directions of a grain are aligned with the global X and Z directions, respectively. Then, an Euler rotation following the Bunge rotation scheme is applied to the grain to obtain the initial orientation of the grain (Fig. 1d). The rotation is identified based on the Euler angle set $\{E\} = \{\varphi_1, \Phi, \varphi_2\}$. φ_1, Φ and φ_2 cause rotation of $[10\bar{1}0]$ in the plane of the sheet, rotation of $[0001]$ away from the sheet normal and the rotation of $[10\bar{1}0]$ out of the plane of the sheet, respectively. For a polycrystalline sample, N_g Euler angle sets are required for each specimen. For each $\{E\}$, normal distributions with zero mean and standard deviation equal to $\{\Delta E\} = \{\Delta\varphi_1, \Delta\Phi, \Delta\varphi_2\}$ respectively are generated. An Euler angle set is formed by randomly picking an Euler angle from its corresponding distribution. The generated texture is identified by $\{\Delta E\} = \{\Delta\varphi_1, \Delta\Phi, \Delta\varphi_2\}$; the pole figures are plotted using the open source package MTEX [8].

The first columns in Figs. 2 and 3 respectively show the initial $[0001]$ and $[10\bar{1}0]$ pole figures for two different values of $\Delta\varphi_2$ keeping $\Delta\varphi_1$ and $\Delta\Phi$ fixed. Increasing $\Delta\varphi_1$ increases the spread of $[10\bar{1}0]$ poles in the plane of the sheet leading to drop in peak intensity. While increasing $\Delta\varphi_2$ does not affect the initial $[0001]$ pole figure, it causes the spread of $[10\bar{1}0]$ poles away from plane of the sheet, which results in a decrease in the peak intensity (Fig. 3).

Crystal Plasticity Model

The crystal plasticity model used here accounts for eighteen (3 basal, 3 prismatic $\langle a\rangle$, 6 pyramidal $\langle a\rangle$ and 6 pyramidal $\langle c+a\rangle$) slip systems and twelve (6 extension and 6

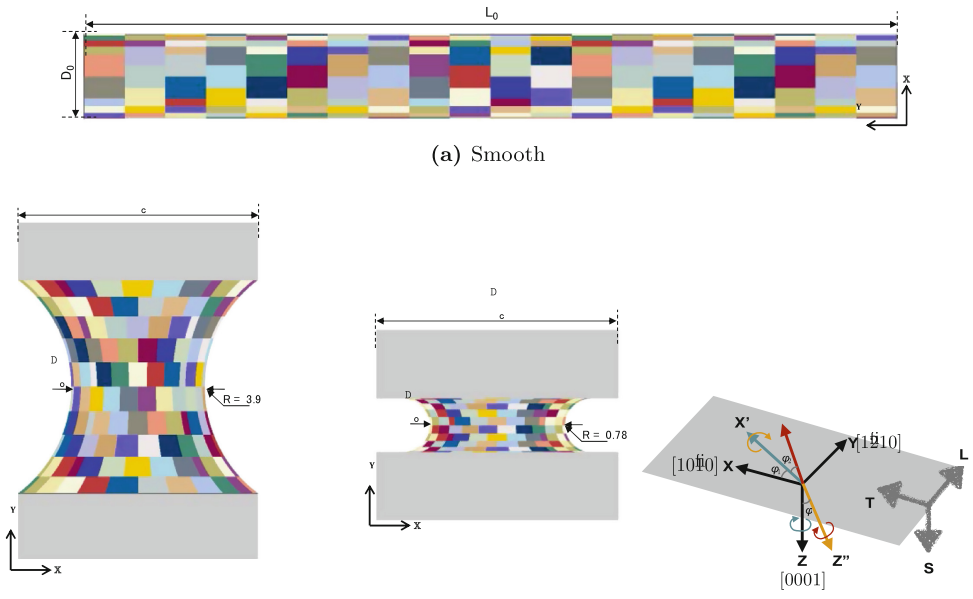

(a) Smooth

(b) RN10

(c) RN2

(d) Texture nomenclature

Fig. 1 **a–c** Smooth and notched polycrystalline specimens. Finite elements of the same color denote a grain. **d** Bunge rotation scheme

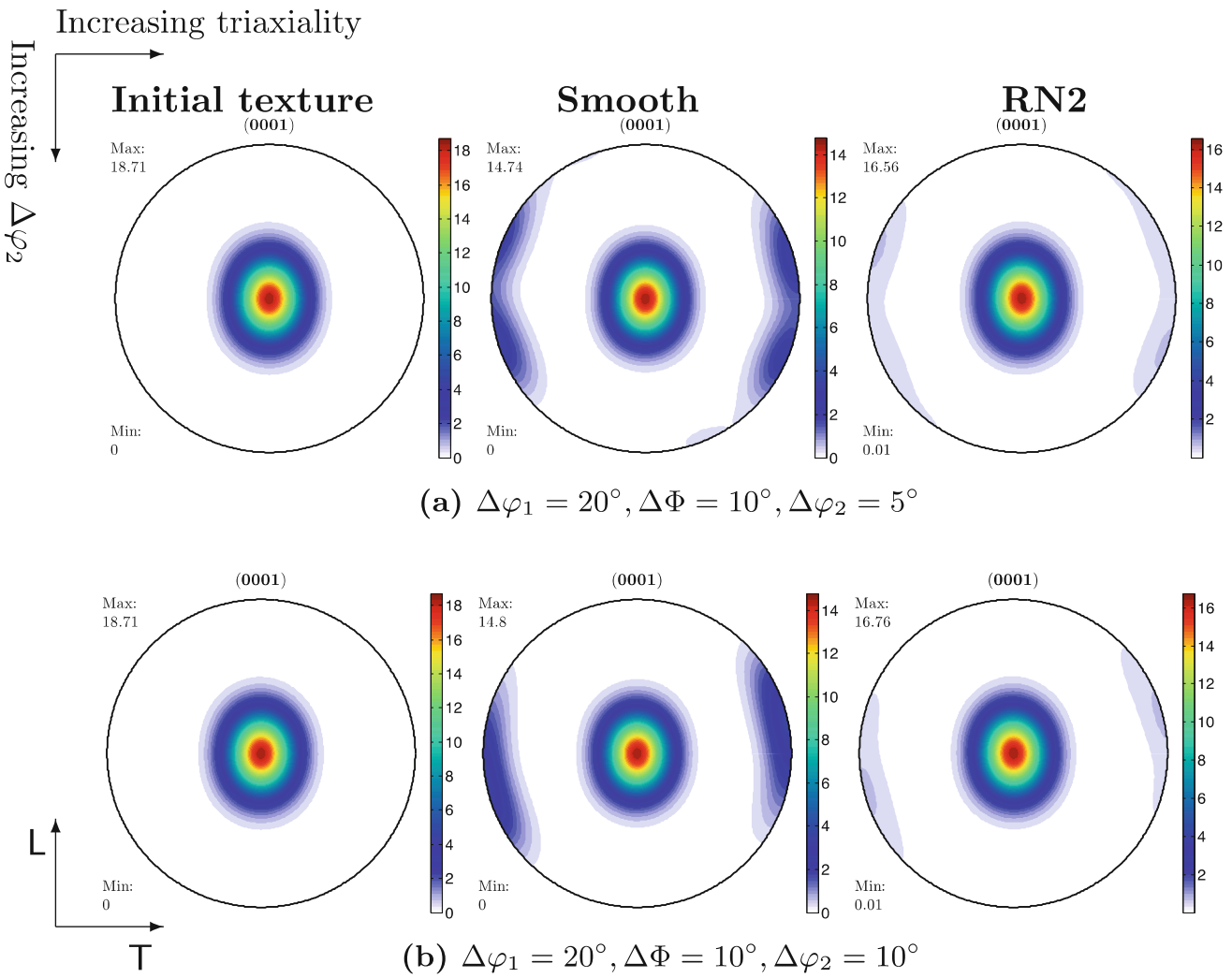

Fig. 2 (0001) pole figures corresponding to initial (column 1) and deformed textures of the smooth (column 2) and RN2 specimens (column 3). Deformed textures are shown at $\varepsilon_A = 0.2$

contraction) twin systems, with physically based hardening laws for self and latent hardening [9].

Here, our focus is on the effect of the distribution of $[10\bar{1}0]$ out of the plane of the sheet, i.e. varying $\Delta\varphi_2$. Two quantities are of interest in this work—(i) macroscopic deformation anisotropy and (ii) micromechanical relative deformation activity. Deformation anisotropy R_L is defined as the ratio of the diametric strain along **T** to the diametric strain along **S**; i.e. $R_L = \varepsilon_{\mathbf{T}}/\varepsilon_{\mathbf{S}}$ where $\varepsilon_\alpha = \ln(D_\alpha/D_0)$ in the direction α; D_α is the current characteristic specimen diameter and D_0 is the initial characteristic diameter; total areal strain $\varepsilon_A = \varepsilon_{\mathbf{T}} + \varepsilon_{\mathbf{S}}$. Relative activity for a given slip/twin system is defined as the ratio of the increment in accrued shear strain on that slip system to the increment in net plastic shear strain.

Results

The specimens are loaded along the sheet rolling direction at a constant nominal strain rate of $1 \times 10^{-3}\,\mathrm{s}^{-1}$. The material parameters for slip and twin systems represent those of an Mg alloy (AZ31) [6]. Figure 4a shows the variation in R_L for different values of $\Delta\varphi_2$ for various specimen geometries considered. The deformation anisotropy increases with increasing $\Delta\varphi_1$ and $\Delta\varphi_2$ while it decreases with increasing notch acuity. For a given in-plane textural variation ($\Delta\varphi_1$), R_L increases with increasing $\Delta\varphi_2$, albeit mildly. While the trends for the smooth and notched specimens are similar, it is clear that the triaxiality has a quantitative effect on R_L, which is also affected by the overall initial texture.

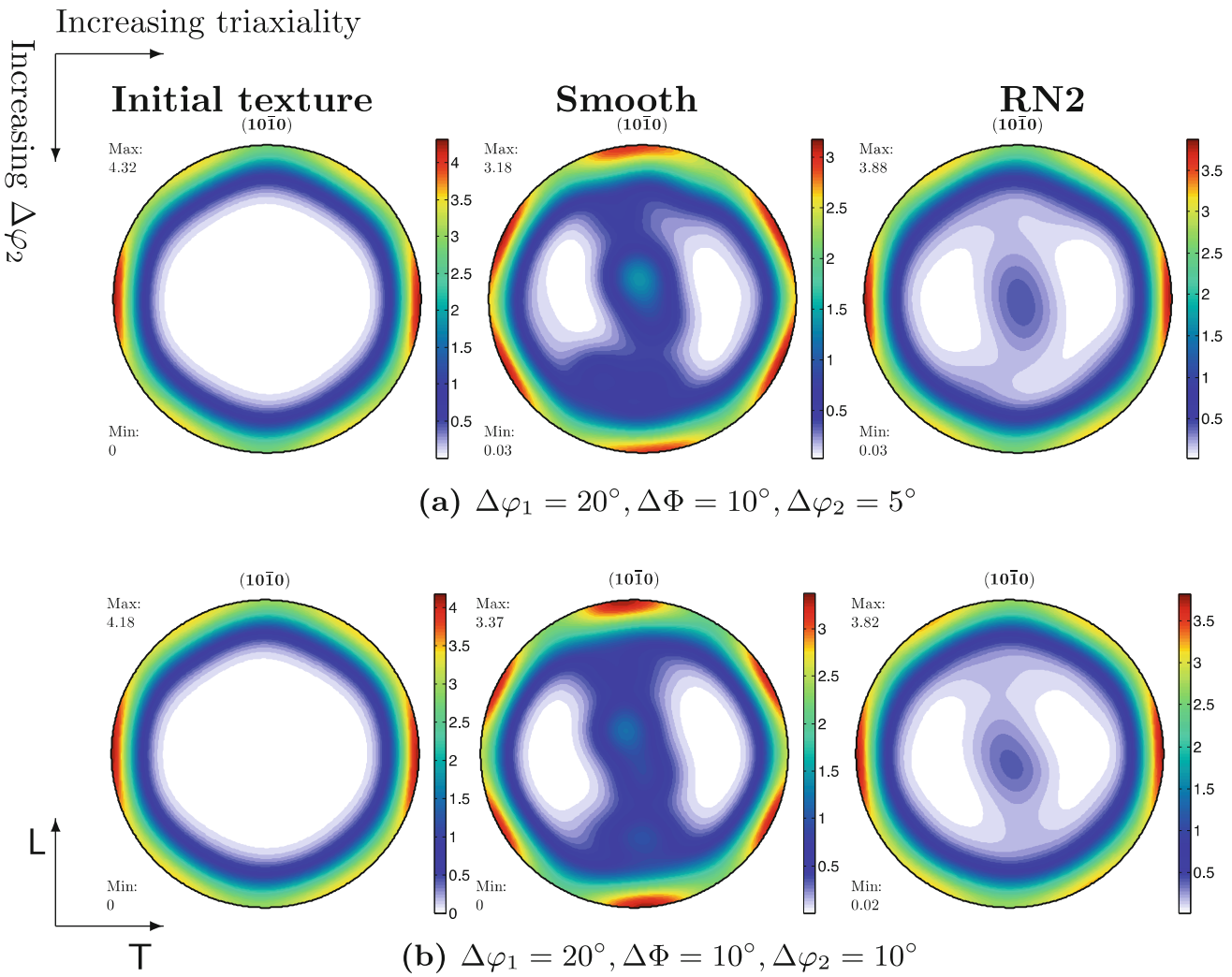

Fig. 3 $(10\bar{1}0)$ pole figures corresponding to initial (column 1) and deformed textures of the smooth (column 2) and RN2 (column 3) specimens. Deformed textures are shown at $\varepsilon_A = 0.2$

The relative activity of key slip modes provide insight into the variation in R_L with $\Delta\varphi_2$. Figure 4b shows the relative activity plots of the prismatic $\langle a \rangle$ and pyramidal $\langle c+a \rangle$ slip modes for different initial textures and nominal triaxialities. Increasing φ_1 and/or φ_2 increase the resolved shear stress (RSS) on the prismatic $\langle a \rangle$ slip systems, which increases their activity, thereby leading to a larger deformation anisotropy. On the other hand, presence of lateral stresses increases in the RSS on the pyramidal $\langle c+a \rangle$ slip planes, which leads to decrease in R_L. In other words, weakening the $[10\bar{1}0]$ texture leads to increase in R_L whereas increasing triaxiality decreases R_L. As seen in Fig. 4c, the importance of basal slip also decreases with increasing φ_2 for a given triaxiality. Note that for a given φ_2 the basal slip becomes more profuse with increasing notch acuity. The analysis shows that increasing basal slip activity causes textural sharpening but its influence is lesser compared to the prismatic slip, discussed *et seq*.

It can be seen that for fixed φ the effect of φ_1 (in-plane variation) on R_L is stronger compared to φ_2. It is useful to consider the limiting case of a single crystal Mg loaded along $[1\bar{2}10]$ with $[10\bar{1}0]$ and $[0001]$ as the transverse directions [6]. Deformation along $[10\bar{1}0]$ is accommodated by prismatic $\langle a \rangle$ and pyramidal $\langle a \rangle$ slip while pyramidal $\langle c+a \rangle$ slip and contraction twinning accommodate the deformation along $[0001]$. Both, pyramidal $\langle a \rangle$ slip and contraction twinning are plastically harder compared to prismatic $\langle a \rangle$ and pyramidal $\langle a \rangle$ slip.

The effect of deformation micromechanics is reflected in the (0001) and $(10\bar{1}0)$ deformed textures (the second and third columns in Figs. 2 and 3), respectively. As seen in the $[0001]$ deformed textures (at a fixed ε_A), peaks occur along

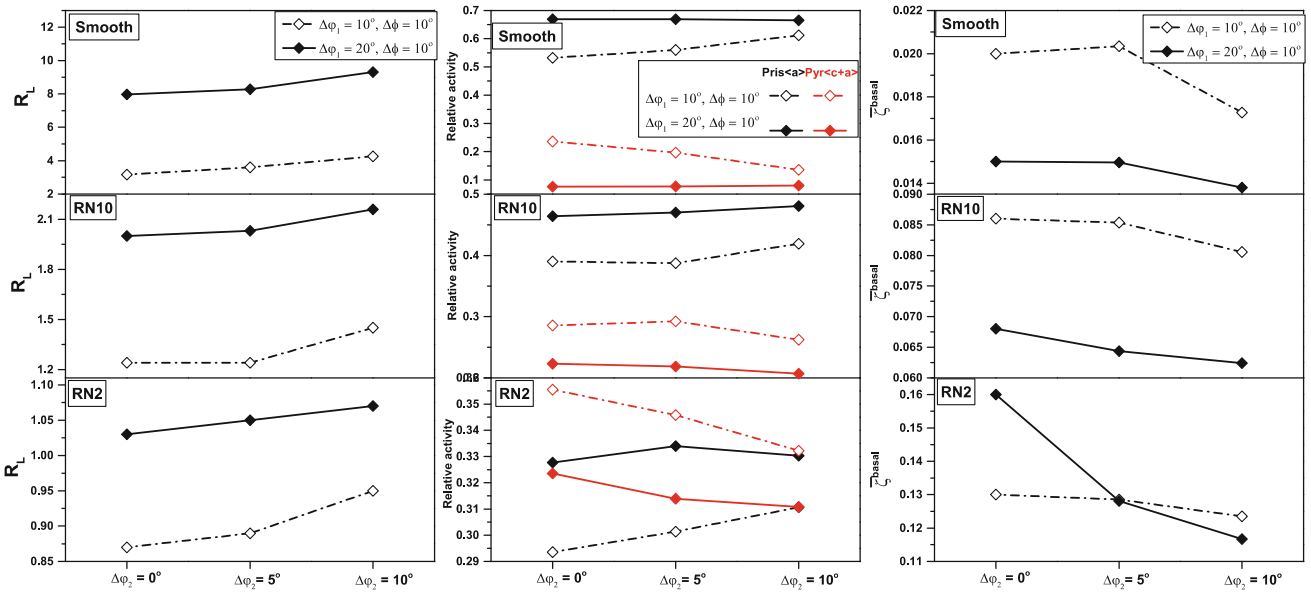

(a) R_L (b) Relative activity (c) Basal slip

Fig. 4 **a** Variation of anisotropy ratio and **b** relative activity of prismatic $\langle a \rangle$ and pyramidal $\langle c+a \rangle$ slip for various values of $\{\Delta E\} = \{\Delta\varphi_1, \Delta\Phi, \Delta\varphi_2\}$ at $\varepsilon_A = 0.1$

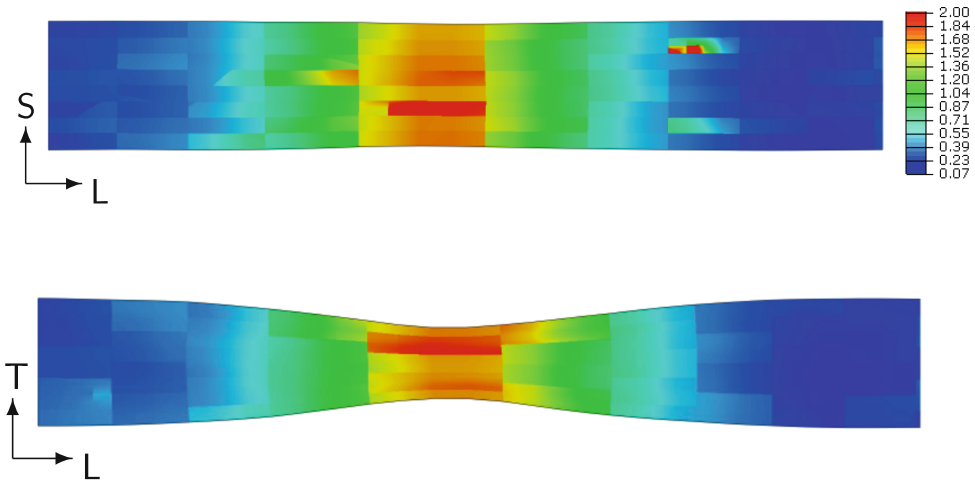

Fig. 5 Cumulative shear at the onset of localization

T and they are more intense in the smooth specimens, for both the φ_2 values, compared to the RN2 specimens (RN10 case in intermediate to these two cases). Similarly, peaks occur in the $(10\bar{1}0)$ textures in the **S** direction (out of the plane of the paper), which are spread out along **L** direction. Again, their intensity is higher in the smooth specimens compared to the RN2 specimens. The peaks occur because of the occurrence of extension twinning, which are found to be present in both, smooth and notched specimens. However, smooth specimens exhibit severe strain localization at $\varepsilon_A = 0.2$ (Fig. 5), which gives rise to more intense twinning, whereas the notched geometries do not show such severe local deformations. However, the quantitative effect is sensitive to the actual amount of twinning that occurs in the specimens, which is in turn determined by the initial texture. In general, increase in φ_2 tends to accelerate localization in smooth specimen, which accelerates twinning in the localized region and therefore, produces more intense textural changes. In the notched specimens, while twinning still occurs (due to the lateral stresses) higher triaxiality tends to suppress localization and therefore, the textural changes are not as dramatic.

Also note the occurrence of six-fold peak intensities of $(10\bar{1}0)$ pole figures in the smooth specimens, which are not present in the initial texture and are also conspicuously absent in the deformed texture of the RN2 specimen. Similar

observations were also reported in our recent work where the effect of φ_2 was not considered and was attributed to unequal straining of prismatic $\langle a \rangle$ systems [7]. Comparing those texture results with the present ones, we infer that the deviation in φ_2 tends to weaken the influence of φ_1 and Φ on the deformed textures. In the presence of triaxiality, the six peaks, indicative of textural sharpening, do not occur because of the reduced relative importance of the prismatic $\langle a \rangle$ slip compared to the pyramidal $c+a$ slip (Fig. 4b).

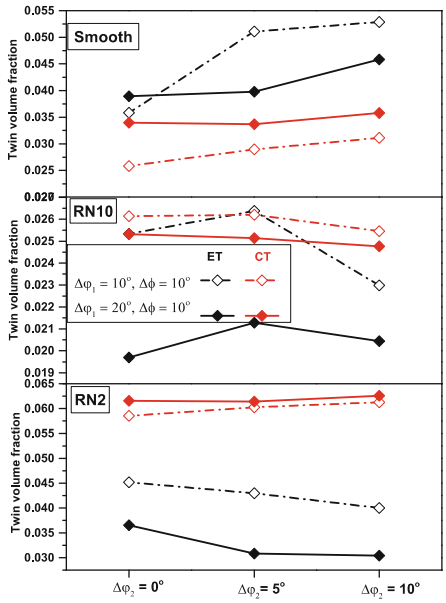

(a) Twin volume fraction

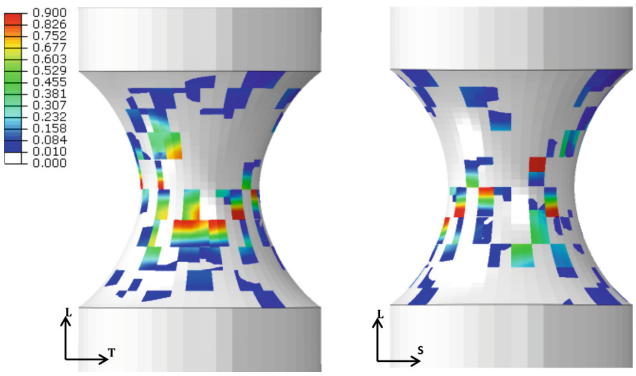

(b) Distribution of extension twins

Fig. 6 **a** Variation of twin volume fraction for all specimens for different $\{\Delta E\} = \{\Delta\varphi_1, \Delta\Phi, \Delta\varphi_2\}$ and **b** distribution of extension twin volume fraction in the RN10 specimen for $\{\Delta E\} = \{20°, 10°, 5°\}, \varepsilon_A = 0.1$

Note however that increasing φ_2 tends to reinstate the importance of prismatic slip, which suggests that textural sharpening to depend on how strongly texture couples into triaxiality. For example, there may be a range of triaxiality over which deviations in φ_2 may not have a strong influence over prismatic slip because other mechanisms may be more dominant.

Figure 6a shows the distribution of twin volume fraction; with increasing $\Delta\varphi_2$, the twin volume fraction increases in the smooth specimen whereas it remains constant or decreases in the notch specimens. Contraction twinning is favored for the given range of initial textures; however extension twinning is also active. Despite unfavorable crystallographic orientation, extension twinning is occurs due to the combined effect of lateral stresses and intergranular stresses arising from misorientation and depends on the intrinsic plastic anisotropy. Figure 6b shows the distribution of twin volume fraction for an RN10 specimen with a particular texture. The twin volume fraction is distributed over the entire volume of the notch. This is different from the observation in single crystals where the twins were confined to certain volume close to the notch root [6]. The detrimental effect of contraction twinning on the ductility of Mg has been long known [1, 10] although the exact effect of extension twinning on ductility is much debated [3, 11, 12]. Nevertheless, taking cognizance of the individual and coupled effects of texture and triaxiality in Mg is essential for understanding damage in Mg.

Conclusion

In this work, we presented the effect of textural variation due to deviations in the $[10\bar{1}0]$ out of the plane of rolled Mg sheets in smooth and notched round bar specimens subjected to tensile loading. In comparison to the $[10\bar{1}0]$ in plane (φ_1) and $[0001]$ out-of-plane (φ) textural variation effects, the deviations in φ_2 result in subtle changes to the macroscopic deformation anisotropy and the underlying microscopic deformation slip and twin activity. The general qualitative effect on textural evolution is that this effect tends to temper the textural sharpening effect induced by φ_1 and φ deviations. Both, extension and contraction twinning mechanisms are active and show complex trend in the texture-triaxiality space.

Acknowledgements BS thanks support through NUS Research Scholarship from Ministry of Education (MoE), Singapore. SPJ is grateful for the support from the US Army's International Technology Center, Pacific (ITC-PAC) through research contract # FA5209-10-P-0047 (R-265-000-338-597). AAB is grateful for the support provided by the National Science Foundation under Grant Number CMMI-1563580.

References

1. B. Kondori, A. Benzerga, Effect of stress triaxiality on the flow and fracture of Mg alloy AZ31. Metall. Mater. Trans. A **45**, 3292–3307 (2014)
2. B. Kondori, A. Benzerga, On the notch ductility of a magnesium-rare earth alloy. Mater. Sci. Eng. A **647**, 74–83 (2015)
3. N.S. Prasad, N.N. Kumar, R. Narasimhan, S. Suwas, Fracture behavior of magnesium alloys—role of tensile twinning. Acta Mater. **94**, 281–293 (2015)
4. V. Kaushik, R. Narasimhan, R.K. Mishra, Finite element simulations of notch tip fields in magnesium single crystals. Int. J. Fract. **189**, 195–216 (2014)
5. M.J. Nemcko, J. Li, D.S. Wilkinson, Effects of void band orientation and crystallographic anisotropy on void growth and coalescence. J. Mech. Phys. Solids **95**, 270–283 (2016)
6. B. Selvarajou, B. Kondori, A.A. Benzerga, S.P. Joshi, On plastic flow in notched hexagonal close packed single crystals. J. Mech. Phys. Solids **94**, 273–297 (2016)
7. B. Selvarajou, S.P. Joshi, A.A. Benzerga, Three dimensional simulations of texture and triaxiality effects on the plasticity of magnesium alloys. Acta. Mater. **127**, 54–72 (2017)
8. F. Bachmann, R. Hielscher, H. Schaeben, Texture analysis with MTEX—free and open source software toolbox. Solid State Phenom. **160**, 63–68 (2010)
9. J. Zhang, S. Joshi, Phenomenological crystal plasticity modeling and detailed micromechanical investigations of pure magnesium. J. Mech. Phys. Solids **60**, 945–972 (2012)
10. E. Kelley, W. Hosford, *The Plastic Deformation of Magnesium*. Technical Report, DTIC Document (1967)
11. H. Somekawa, A. Singh, T. Mukai, Fracture mechanism of a coarse-grained magnesium alloy during fracture toughness testing. Philos. Mag. Lett. **89**, 2–10 (2009)
12. V. Kaushik, R. Narasimhan, R. Mishra, Experimental study of fracture behavior of magnesium single crystals. Mater. Sci. Eng. A **590**, 174–185 (2014)